Engineering Applications of Artificial Intelligence 133 (2024) 108010

Contents lists available at ScienceDirect

Engineering Applications of Artificial Intelligence

journal homepage: www.elsevier.com/locate/engappai

A novel damage identification algorithm by combining the boundary element method and a series connection neural network

Yang Yang [a,b,*], Zheng Zhan [b], Yijun Liu [b]

[a] Faculty of Material Science, Shenzhen MSU-BIT University, Shenzhen, Guangdong, 518172, China
[b] Department of Mechanics and Aerospace Engineering, Southern University of Science and Technology, Shenzhen, Guangdong, China

ARTICLE INFO

Keywords:
Novel damage identification
Model driven
Data driven
Boundary element method
Neural network

ABSTRACT

A novel damage identification approach based on a model-driven and a data-driven combined algorithm is developed. By using this approach with only boundary strains, the existence, location, classification as well as the extent of the damage in a plate can be predicted at once with high accuracy and efficiency. To accumulate the data, the boundary element method (BEM) is applied as a model-driven in modeling plates with one or multiple damages in the forms of circular or elliptical holes or cracks and for solving the boundary strains of the defective plates. The dimensionality reduction and semi-analytical characteristics of BEM not only can compress the feature data also can improve the accuracy of the database for the data-driven algorithm. The boundary strains are obtained directly from BEM models, which are also easily collected through the use of strain gauges mounted on the surfaces of structures being monitored in real applications. A series connection neural network algorithm is established to accomplish the novel damage identification assignments with deep learning. The number of the existing damages is firstly detected by a classification neural network model, then the extracted features are transmitted to the corresponding regression neural network model to prognosis the location, classification as well as the extent of each flaw. A high accuracy of about 99.86 % is achieved by the present combined neural network algorithm, which is promising in applications of actual structural health monitoring.

1. Introduction

Structural health monitoring (SHM) has become an important technique in the field of disaster prevention and mitigation for civil, aerospace, and mechanical engineering (Figueiredo et al., 2011). A five-step hierarchy is typically considered in SHM: First, identification of the damage existence; Second, detection of the damage location; Third, distinguishing of the damage classification; Fourth, recognition of the damage extent; And last, prediction of the remaining life of the structure (Malekloo et al., 2022). Among them, the first four steps belong to the category of damage identification. Thus, damage identification is the key technique in SHM. In the past, identifying damage was only based on a periodic inspection either carried out using non-destructive evaluation (NDE) or by visual observation. Nowadays, offline damage identification has been replaced with near real-time and online damage assessment. In recent two decades, damage identification has been performed mainly based on two independent approaches: model-based and data-based (Farrar and Worden, 2007).

The model-based approaches are rooted in techniques based on finite element (FE) model updating (Sohn et al., 2003). These techniques aim at identifying structural damage by comparing the measured response of the structure with a baseline FE model, tailored for that specific structure and validated against its undamaged behavior (Cao et al., 2018) (Wang et al., 2020). Considerable uncertainty is inherent to FE model updating including both the random occurrences associated with experimental readings of the structural response and the uncertainties associated with the FE discretization (Moore et al., 2012). These uncertainties shift the model-based SHM from deterministic to probabilistic. Furthermore, the model-based approaches cannot achieve the five-step hierarchy damage identification (Kassab et al., 1994). Damage identification is an inverse problem in mechanics. These inverse problems are complicated because of the difficulty of the measured conditions, the ill-posed equations, the complexity of the solution processes, and the unusual nature of the inverse problem, which make it more difficult to calculate the relevant physical quantities by numerical methods. Except for the FEM, the boundary element method (BEM) (Yang et al., 2015) (Liu, 2009) and extended finite element method (XFEM) (Jung and Taciroglu, 2014) also have been applied to deal with

* Corresponding author. Faculty of Material Science, Shenzhen MSU-BIT University, Shenzhen, Guangdong, 518172, China.
E-mail address: yangy2023@smbu.edu.cn (Y. Yang).

https://doi.org/10.1016/j.engappai.2024.108010
Received 7 November 2023; Received in revised form 13 January 2024; Accepted 29 January 2024
Available online 7 February 2024

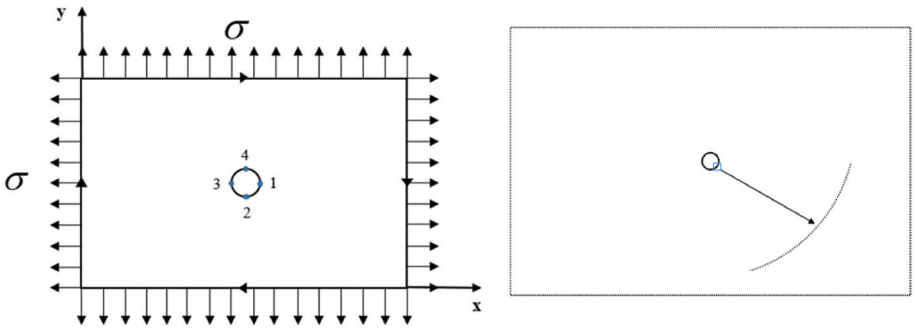

Fig. 1. A plate subjected a remote tensile stress with a center circular hole.

Table 1
Verification of the stresses of the four points on the circular hole.

Point	σ_x	σ_y	τ_{xy}	$\sigma_E(BEM)$	$\sigma_E(Exact)$	Error (%)
1	0.0000	2.0142	0.0000	2.0142	2.0	0.71
2	2.0050	0.0000	0.0000	2.0050	2.0	0.25
3	0.0000	2.0142	0.0000	2.0142	2.0	0.71
4	2.0050	0.0000	0.0000	2.0050	2.0	0.25

some damage identification work (Mellings and Aliabadi, 1993) (Sun et al., 2016), but their efficiency is restricted by some limitations.

Conversely, approaches based on data models with machine learning algorithms (MLAs) are developed quickly to separate changes in the damage-sensitive features caused by structural damage (Zhang, 2007) (Yang et al., 2023). Several MLAs with different working principles have been proposed in the last two decades (Sun et al., 2020)- (Bolandi et al., 2022). They can probably be divided into two categories. The first kind is supervised learning algorithms including Decision Tree (DT) (Mariniello et al., 2020), Random Forest (RF) (Lu et al., 2020), Support Vector Machine (SVM) (Bigoni and Hesthaven, 2020), k-nearest Neighbor (Salehi et al., 2019) and Bayesian (Lee and Song, 2016); The other is based on unsupervised learning algorithms including K-means (Alamdari et al., 2017), Association analysis (Jin et al., 2019) and Blind Source Separation (BSS) (Yang et al., 2017). Last but not least is Neural Network (NN), which is considered as a supervised or unsupervised learning approach (Fang et al., 2005). NN approaches in damage detection are similar to the working components in a human brain. It has been widely used in earlier works (Hekmati Athar et al., 2020) (Jagtap et al., 2020). Among these data-driven approaches, the first step of the damage identification hierarchy can be achieved by virtually every ML technique. The second and the fourth steps are also considered in most of

Table 2
Verification of the stresses of the four points on the elliptical hole.

Node	σ_x	σ_y	τ_{xy}	$\sigma_E(BEM)$	$\sigma_E(Exact)$	Error(%)
1	0.0000	4.0250	0.0000	4.0250	4.0	0.63
2	0.9918	0.0000	0.0000	0.9918	1.0	0.82
3	0.0000	4.0252	0.0000	4.0252	4.0	0.63
4	0.9918	0.0000	0.0000	0.9918	1.0	0.82

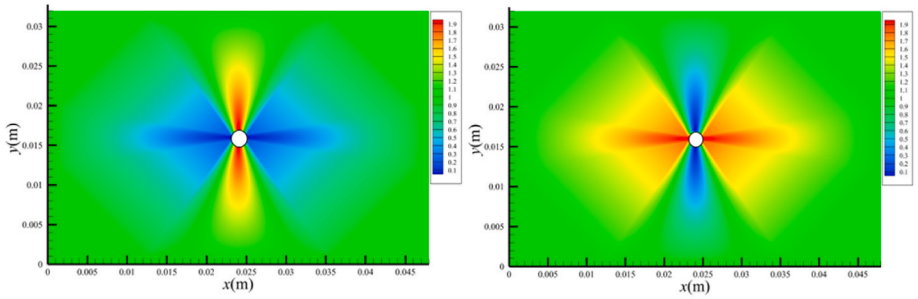

(a) (b)

Fig. 2. Stress contour plots of Case 1: (a) σ_x and (b) σ_y.

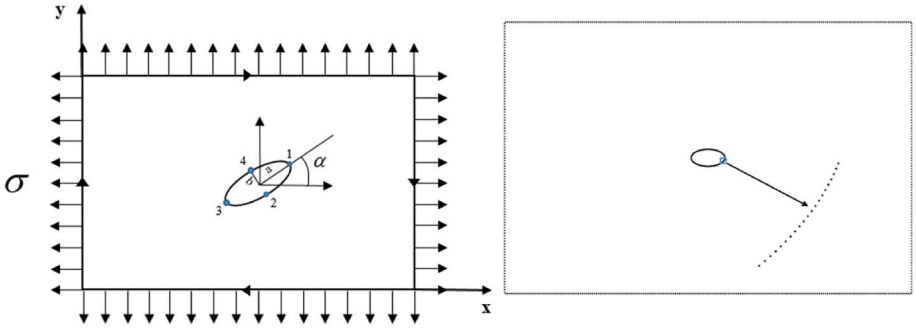

Fig. 3. A plate subjected to a remote tensile stress with a center elliptical hole.

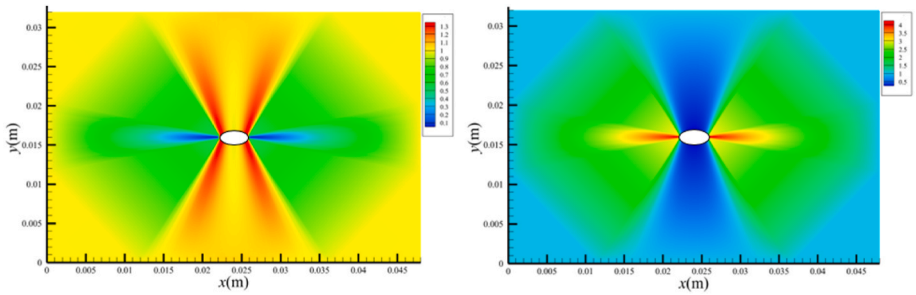

Fig. 4. Stress contour plots of Case 2: (a) σ_x and (b) σ_y.

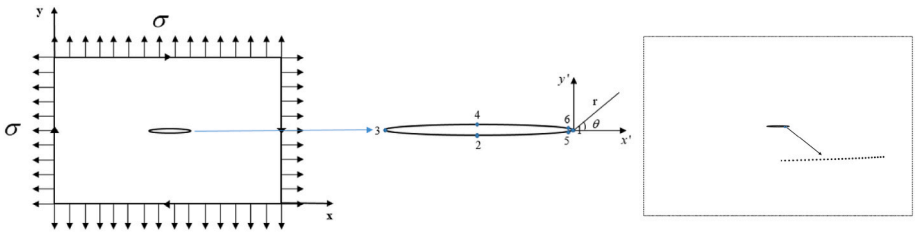

Fig. 5. A plate subjected to a remote tensile stress with a center crack.

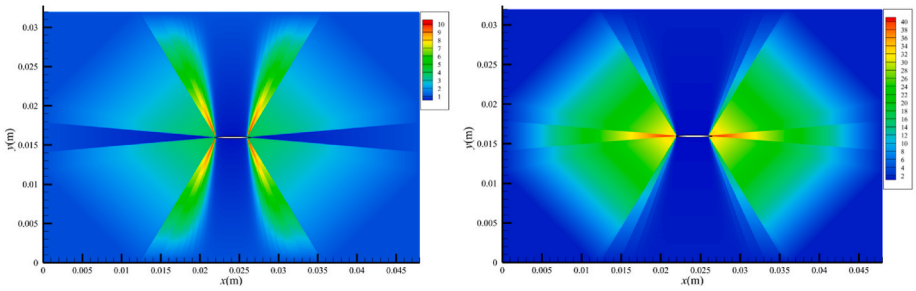

Fig. 6. Stress contour plots of Case 3 (a) σ_x, (b) σ_y

Table 3
Verification of the stresses of the one to four points on the crack.

Node	σ_x	σ_y	τ_{xy}	$\sigma_E(BEM)$	$\sigma_E(Exact)$	Error (%)
1	0.0000	40.4491	0.0000	40.4491	40.0	1.12
2	0.1009	0.0000	0.0000	0.1009	0.1	0.90
3	0.0000	40.4491	0.0000	40.4491	40.0	1.12
4	0.1009	0.0000	0.0000	0.1009	0.1	0.90

the applications. However, many works did not either take into account the third and the fifth steps or believed that the algorithms were not suitable or capable for damage classification and prognosis. Only the algorithm of neural network can achieve all the five levels. Nevertheless, in the future, a more in-depth assessment of damage classification should be studied.

For the data-driven based method, a generalizability, fairness and scientific validity dataset is one of the essential prerequisites. However, the dataset is hardly collected totally from the operational engineering systems or experiments due to the long cycles and high costs. Most engineering structures, such as bridges, aircraft, wind turbines, are systems dictated by the size and physical environment in which they are put in service, which challenges the existence of data from all operational and environmental conditions. In addition, due to the one-of-a-kind nature of such structures, it is more difficult to incorporate lessons learned from other normal response patterns throughout their service lifetime. Therefore, a hybrid damage identification approach aimed at combining the best features of model- and data-based algorithms have emerged (Li and Yang, 2008) (Gonzalez and Zapico, 2008). In the hybrid algorithm, the FE model is seen not only as an instrument for exploring the possible causes of past changes in the structural response, but also as a tool for designing an optimal SHM sensor network and a data-base creator to construct the training data for data-based damage-detection algorithms (Mitusch et al., 2021). Although the FE models have been shown to hold considerable potential for optimizing small sensing networks, the number of runs required for a large-scale structure is most often prohibitive (Ku et al., 2023).

Compared with the FE model, the boundary element (BE) model only needs to have the structure boundaries divided into elements, reducing the dimension of the considered model by one. This will directly lead to reduce the number of feature data in sensing networks to a great extent.

Table 4
Verification of the stresses and displacements of five and six points on the crack.

Node	x/mm	y/mm	$\sigma_x(BEM)$	$\sigma_x(Exact)$	$Error\_\sigma_x(\%)$	v(BEM)	v(Exact)	Error_v (%)
5	25.9923	15.9913	3.4146	3.4227	0.24	−0.2440	−0.2473	1.33
6	25.9923	16.0087	3.4164	3.4227	0.18	0.2438	0.2473	1.42

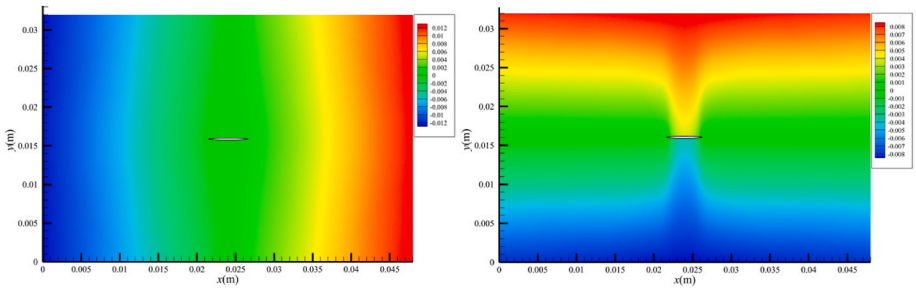

Fig. 7. Displacement contour plots of Case 3 (a) u_x, (b) u_y

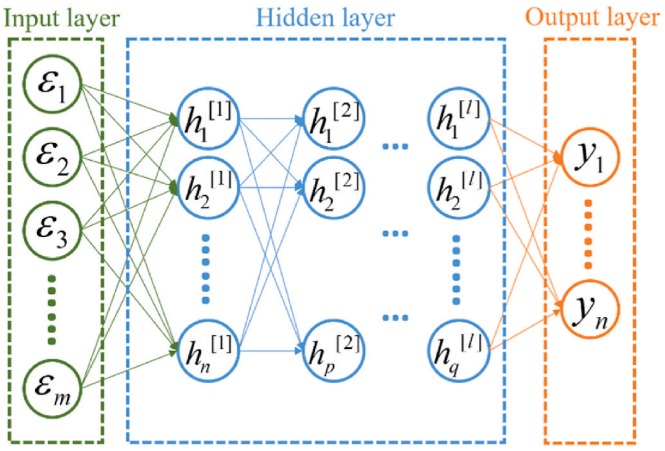

Fig. 8. The configuration of the DNN.

The semi-analytical characteristic of the BE model can obtain a higher accuracy numerical result, which can ensure the quality of data used to optimize the sensing networks. Thus, the conjunction of the BE model with NN to implement the damage identification of structures will be a more efficient strategy (Sun et al., 2022), and its feasibility has been verified by the authors (Han et al., 2022). In our approach, the BEM is applied in modeling the defective structures and in solving the boundary strains. Numerous BEM models and results are composed to form the database for machine learning, which is similar to the collected data through the use of strain gauges mounted on the surfaces of structures being monitored in real applications. Compared with the previous paper where the developed algorithm can only identify the location and extent of one circular hole (Han et al., 2022). A more general algorithm is developed in this work to implement the four-step hierarchy damage identifications. Multiple damages with more complicated forms are considered in the BEM. The single regression NN model has been replaced by a series connection NN model which is composed of classification and regression NNs. A complete four-step hierarchy damage identification for plates with one or multiple damages in the forms of circular or elliptical holes, or cracks can be predicted accurately by the developed algorithm.

The paper is organized as follows. The methodologies of BEM used in model-driven and a serious neural network used in data-driven are presented in a great detail in section 2. Six examples are investigated in Section 3 to demonstrate the accuracy, efficiency and generality of the present NN models. Last Section 4 concludes the advantages and some defects of the present method.

2. Methodology

A coupled approach of the BE model-driven and NN data-driven algorithm can work together to achieve a reasonable level of accuracy in damage identification. Augmentation of data-driven damage identification systems with the BEM can generate labeled datasets for training validation and testing phases. Data compression by means of dimensionality reduction is one of the important stages and is achieved using the BEM. The reduction in the quantity of data set does not reduce the data quality due to the semi-analytical nature of the BEM. Then, a series connection NN model is developed to construct the exact mapping relationship between deformation and configuration of the structure to accurately predict the damage detection, location, classification and extent.

2.1. Database construction by using the boundary element models

In this analysis, the 2D elastostatic BEM (accelerated by the fast multipole method (Liu, 2009)) is applied to solve the problem of a plate with flaws subjected to remote stress loading. The considered domain of the plate is $\Omega \in \mathbb{R}^2$ with boundary S and unit outward normal n. The equilibrium equations and stress-strain relations are given by:

$$\sigma_{ij,j} = 0 \tag{1}$$

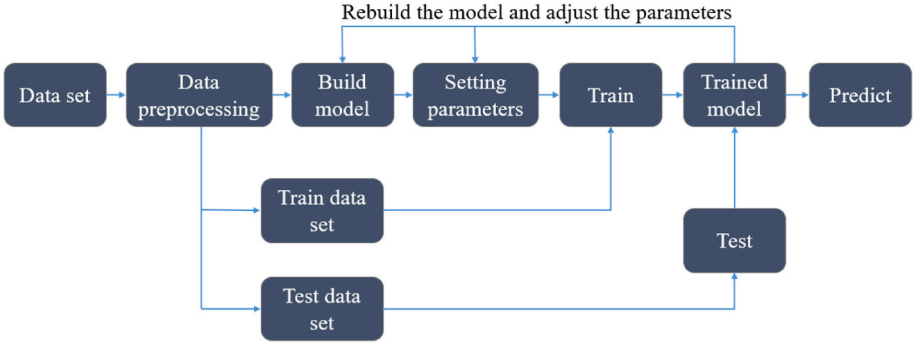

Fig. 9. The training process of DNN model.

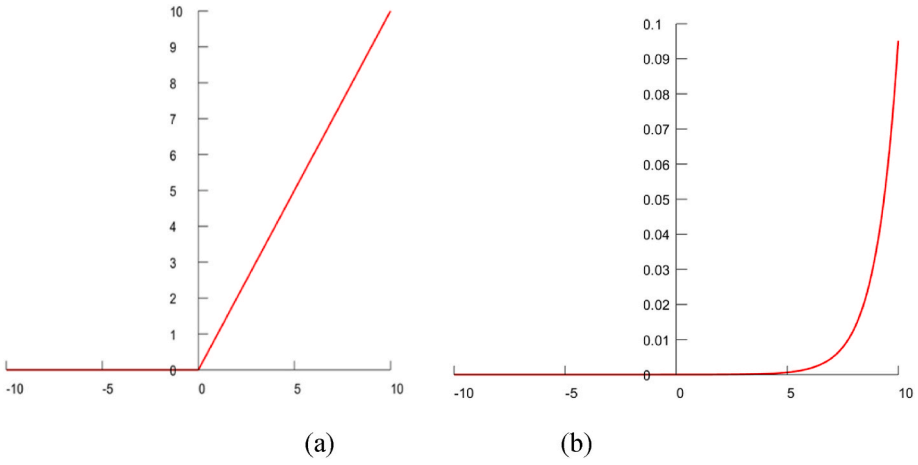

Fig. 10. Images of activation functions (a) ReLU, (b) Softmax.

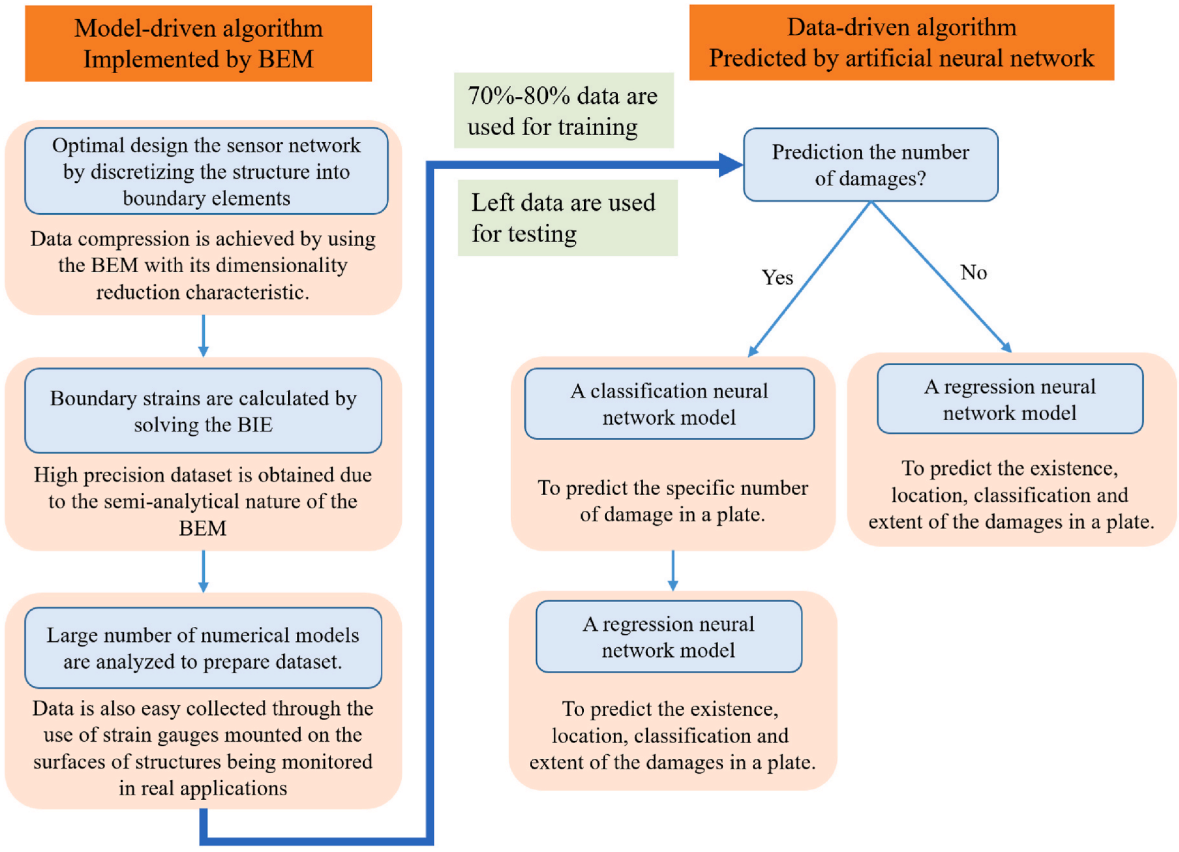

Fig. 11. Flowchart of the present algorithm.

$$\varepsilon_{ij} = \frac{1}{E}\left[(1+\nu)\sigma_{ij} - \nu\sigma_{kk}\delta_{ij}\right] \tag{2}$$

respectively, in which σ_{ij} and ε_{ij} are the stress and strain tensors, δ_{ij} is the Kronecker delta symbol, E is the Young's modulus and ν is the Poisson's ratio of the material. In elastostatic problems, the above equations need to be solved under given boundary constraints and load conditions. By applying the generalized Green's identity and Gauss divergence theorem, the boundary integral equation (BIE) (Liu, 2009) can be established as follows:

$$c_{ij}u_i(\mathbf{x}) = \int_S \left[U_{ij}(\mathbf{x},\mathbf{y})t_j(\mathbf{y}) - T_{ij}(\mathbf{x},\mathbf{y})u_j(\mathbf{y})\right]dS(\mathbf{y}), \forall \mathbf{x} \in S \tag{3}$$

which can be applied to solve for the unknown boundary values of displacements and tractions using the BEM. In BIE (3), U_{ij} and T_{ij} are two kernel functions from the Kelvin's solution (Liu, 2009), and c_{ij} is a coefficient related to the shape of the boundary at point $\mathbf{x}$ ($c_{ij} = 1/2$ for a smooth boundary at $\mathbf{x}$).

By discretizing the boundaries of the domain with constant elements, BIE (3) leads to the following linear system of equations:

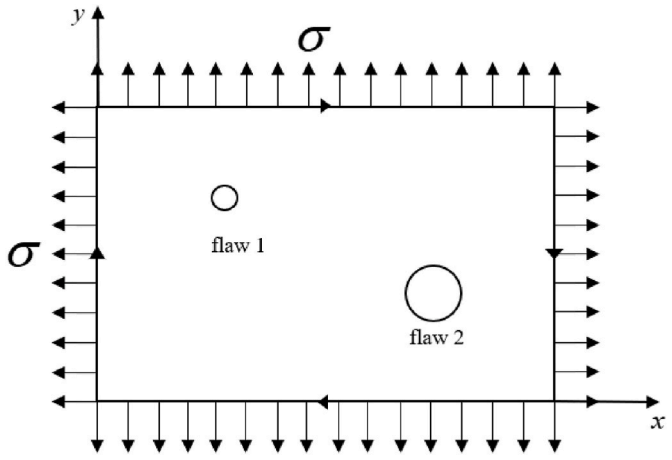

Fig. 12. Two random circular holes in a plate subjected to remote stress.

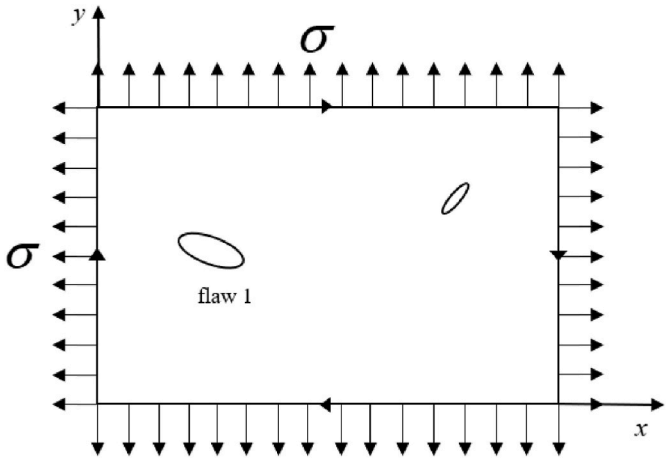

Fig. 15. Two random elliptical holes in a plate subjected to remote stress.

Table 5
NN parameters for example one.

Hidden layer number	Number of neurons	Parameters to be trained	Iterative steps	Loss value/ cm	Training time/s
3	64-64-32	83814	300	0.03087	37

Table 6
NN parameters for example two.

Hidden layer number	Number of neurons	Parameters to be trained	Iterative steps	Loss value	Training time/s
3	128-64-32	165418	300	0.0076	70

$$\mathbf{Hu} = \mathbf{Gt} \tag{4}$$

where **u** and **t** are the displacement and traction vectors, respectively, **H** and **G** are the associated matrices from integration of the kernel functions on all elements. Substituting the boundary conditions into the linear system of equations, the unknown displacements **u** and tractions **t** can be solved by rearranging the unknowns to left-hand-side of the equations, leading to a standard linear system of equations:

$$\mathbf{Ax} = \mathbf{b} \tag{5}$$

Once the values of all boundary displacement and traction are known, the values of the full stresses and strains on the boundary of the domain can be obtained through the following linear system of equations (Liu, 2009):

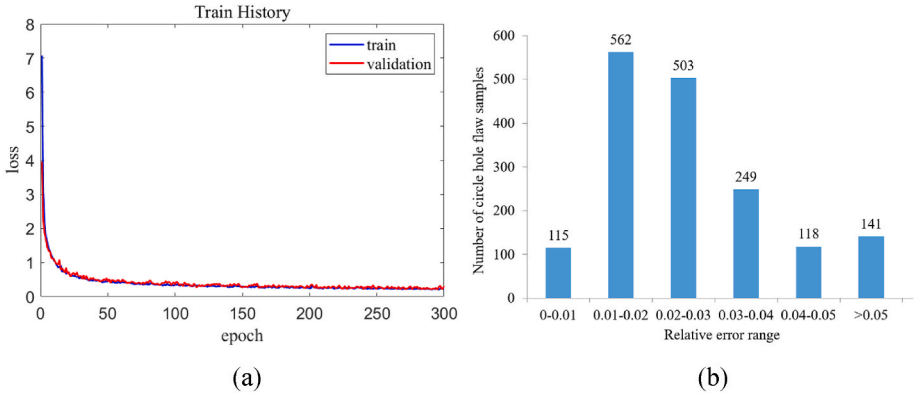

Fig. 13. Loss value results of example one NN model (a) convergence process, (b) distribution of testing samples.

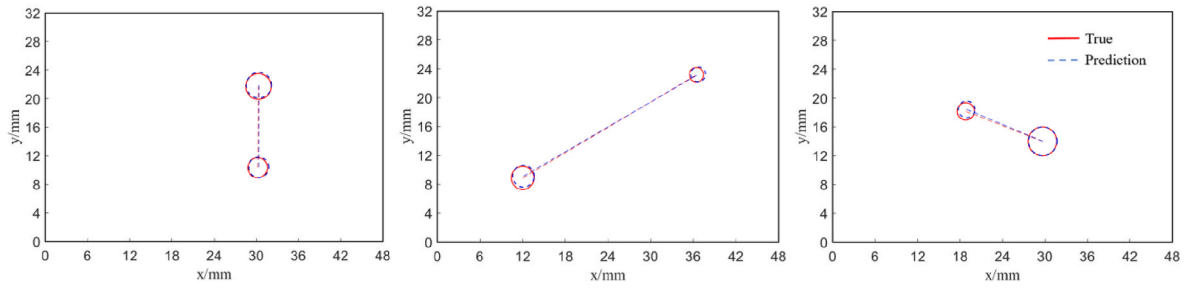

Fig. 14. Comparison between the true and prediction values for two circular holes.

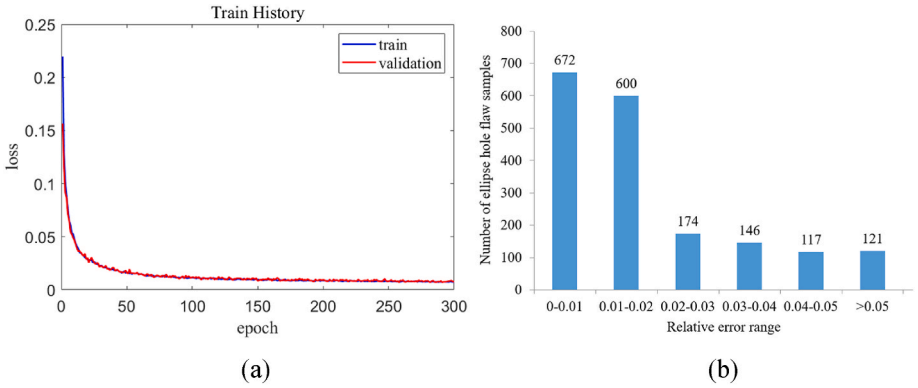

Fig. 16. Loss value results of example two NN model (a) convergence process, (b) distribution of testing samples.

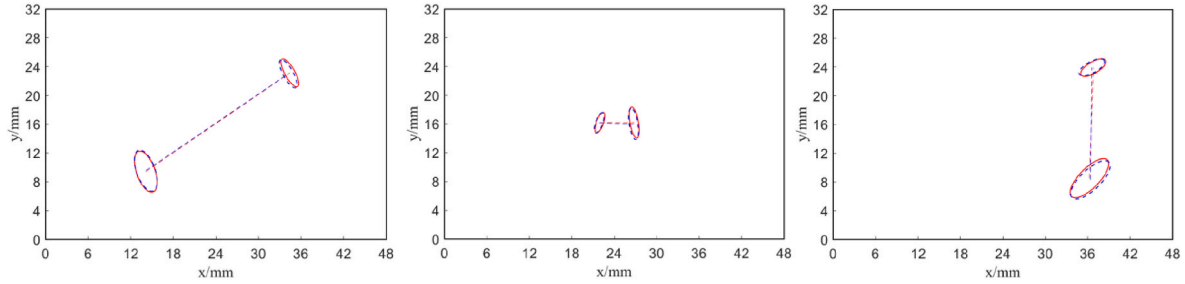

Fig. 17. Comparison between the true and prediction values for two elliptical holes.

$$\begin{bmatrix} n_x & 0 & n_y & 0 & 0 & 0 & 0 \\ 0 & n_y & n_x & 0 & 0 & 0 & 0 \\ 0 & 0 & 0 & \frac{\partial x}{\partial \xi} & \frac{\partial y}{\partial \xi} & 0 & 0 \\ 0 & 0 & 0 & 0 & 0 & \frac{\partial x}{\partial \xi} & \frac{\partial y}{\partial \xi} \\ 1 & 0 & 0 & -C(1-\nu) & 0 & 0 & -C\nu \\ 0 & 1 & 0 & -C\nu & 0 & 0 & -C(1-\nu) \\ 0 & 0 & 1 & 0 & -G & -G & 0 \end{bmatrix} \begin{Bmatrix} \sigma_x \\ \sigma_y \\ \tau_{xy} \\ \frac{\partial u}{\partial x} \\ \frac{\partial u}{\partial y} \\ \frac{\partial v}{\partial x} \\ \frac{\partial v}{\partial y} \end{Bmatrix} = \begin{Bmatrix} t_x \\ t_y \\ \frac{\partial u}{\partial \xi} \\ \frac{\partial v}{\partial \xi} \\ 0 \\ 0 \\ 0 \end{Bmatrix} \tag{6}$$

in which, constant $C = E/[(1+\nu)(1-2\nu)]$ and G is the shear modulus.

The accuracy in prediction of the coupled system depends on the accuracy of the data generated using the BEM models. Thus, the accuracy of the BEM models should be verified first. In this section, three benchmark examples are investigated to verify the accuracy of the BEM models. A plate subjected a remote tensile stress on the four edges and with a center flaw in the form of a circular, elliptical hole or a crack is analyzed by using the BEM models. The effective von-Mises stress for this plane stress problem is expressed as:

$$\sigma_E = \frac{1}{\sqrt{2}}\sqrt{(\sigma_x - \sigma_y)^2 + \sigma_x{}^2 + \sigma_y{}^2 + 6\tau_{xy}{}^2} \tag{7}$$

The rectangular plate considered has a length of 48 mm and a width of 32 mm, and is subjected to a tensile loading $\sigma = 1$ Pa along the four edges. In all cases, the material properties of the plate used are: Young's modulus $E = 1$Pa, Passion's ratio $\nu = 0.3$.

Case 1. A plate with a circular hole

A circular hole with radius 1 mm in the center of the studied plate is plotted in Fig. 1. The analytical values of the stresses of the points on the edge of the circular hole as shown in Fig. 1 are given by (Xu, 2016):

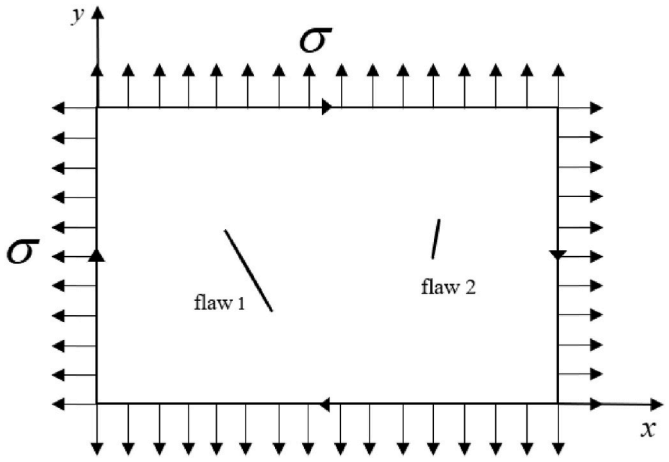

Fig. 18. Two random cracks in a plate subjectetoon remote stress.

Table 7
NN parameters for example three.

Hidden layer number	Number of neurons	Parameters to be trained	Iterative steps	Loss value	Training time/s
3	128-64-32	165352	300	0.0078	58

$$\sigma_{1,2,3,4} = 2\sigma \tag{8}$$

By conducting the convergence study, it is found that 604 and 100 constant elements are needed to discretize the four edges of the plate and the edge of the circular hole, respectively, in order to ensure the accuracy of the BEM results. Four points on the circular hole as shown in Fig. 1 are taken as the samples to carry out the verification. The errors

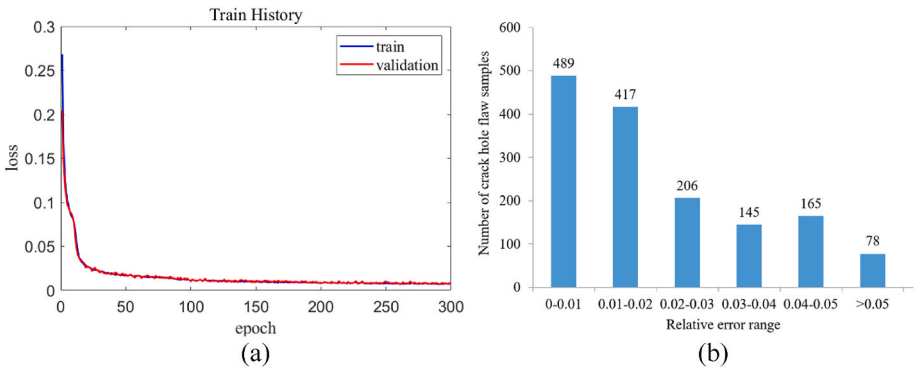

Fig. 19. Loss value results of example three NN model (a) convergence process, (b) distribution of testing samples.

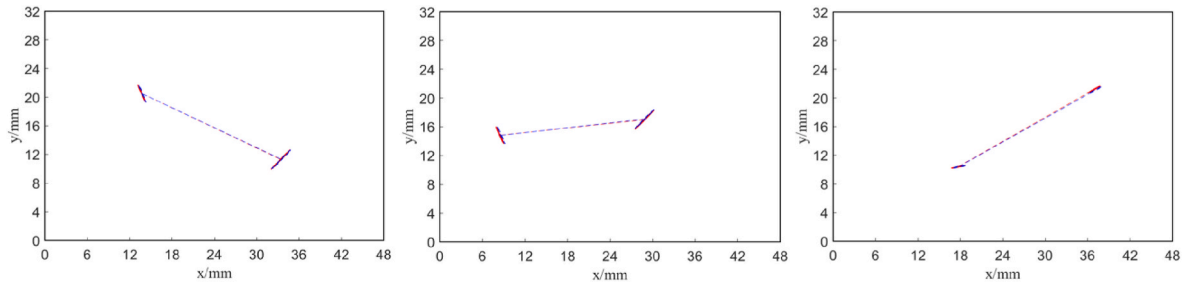

Fig. 20. Comparison between the true and prediction values for two cracks.

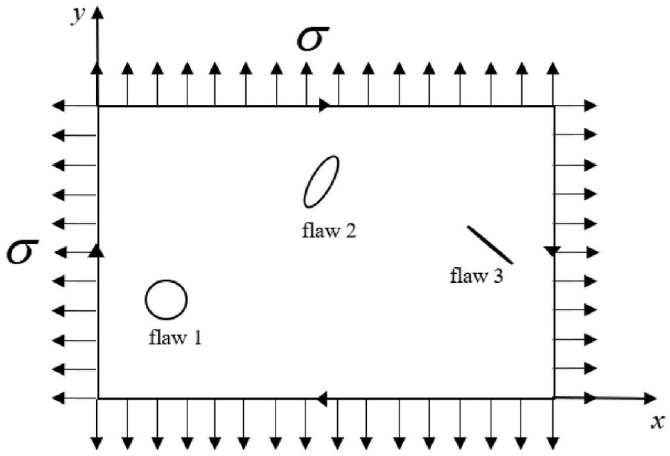

Fig. 21. Three random flaws in a plate subjected to remote stress.

Table 8
NN parameters for example four.

Hidden layer number	Number of neurons	Parameters to be trained	Iterative steps	Loss value	Training time/s
4	256-128-64-32	353231	300	0.0084	84

between the BEM solution and the analytical solution at these four points are listed in Table 1. The developed BEM model is proved to be very accurate, with the relative errors being less than 1 %. The corresponding stress contour plots of the BEM model are depicted in Fig. 2.

Case 2. A plate with an elliptical hole

An elliptical hole in the center of the studied plate is plotted in Fig. 3. The semi-long and short axes of the elliptical are $a = 2mm$ and $b = 1mm$, respectively. The angle θ between the long axis and x-axis is 0. The same as in Case 1, 604 and 100 uniformly distributed constant elements are used on the four edges of the plate and the edge of the elliptical hole, respectively. Four points on the elliptical hole as shown in Fig. 3 are taken as the samples to carry out the verification. The analytical solution of stresses at the four points on the elliptical hole are given by (Xu, 2016):

$$\begin{cases} \sigma_{1,3} = \dfrac{2a}{b}\sigma, \\ \sigma_{2,4} = \dfrac{2b}{a}\sigma. \end{cases} \tag{9}$$

The errors between the BEM and the analytical solution are listed in Table 2. The developed BEM is proved exactly by the relatively small errors. The corresponding stress contour plots of the BEM are depicted in Fig. 4.

Case 3. A plate with a crack

When the short axis approaches to 0, the elliptical hole changes to be a crack with aggravated stress concentration at the crack tip. The same meshes are used to discretize the structure as depicted in Figs. 5 and 6 points are sampled to verify the accuracy of the model. The numerical results of 1–4 points are still compared with the analytical solutions of Eq. (8). The stresses and displacements of two auxiliary points 5 and 6 are verified by the analytical solution given by (Xu, 2016):

$$\begin{cases} \sigma_x = \dfrac{K_{\mathrm{I}}}{\sqrt{2\pi r}}\cos\dfrac{\theta}{2}\left(1 - \sin\dfrac{\theta}{2}\sin\dfrac{3\theta}{2}\right) \\ v = \dfrac{K_{\mathrm{I}}}{G(1+\mu)}\sqrt{\dfrac{r}{2\pi}}\sin\dfrac{\theta}{2}\left[2 - (1+\mu)\cos^2\dfrac{\theta}{2}\right] \end{cases} \tag{10}$$

The comparisons between numerical results and analytical solutions are shown in Tables 3 and 4 which prove the high accuracy of the BE model. The contour plots of stress and displacement of this case are plotted in Figs. 6 and 7, respectively.

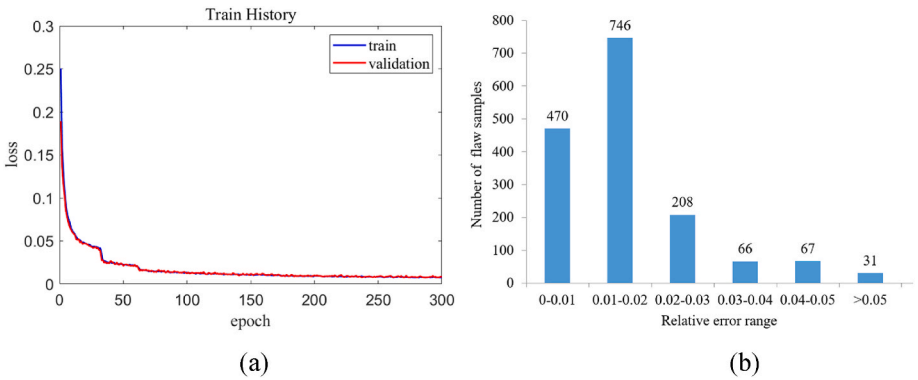

Fig. 22. Loss value results of example four NN model (a) convergence process, (b) distribution of testing samples.

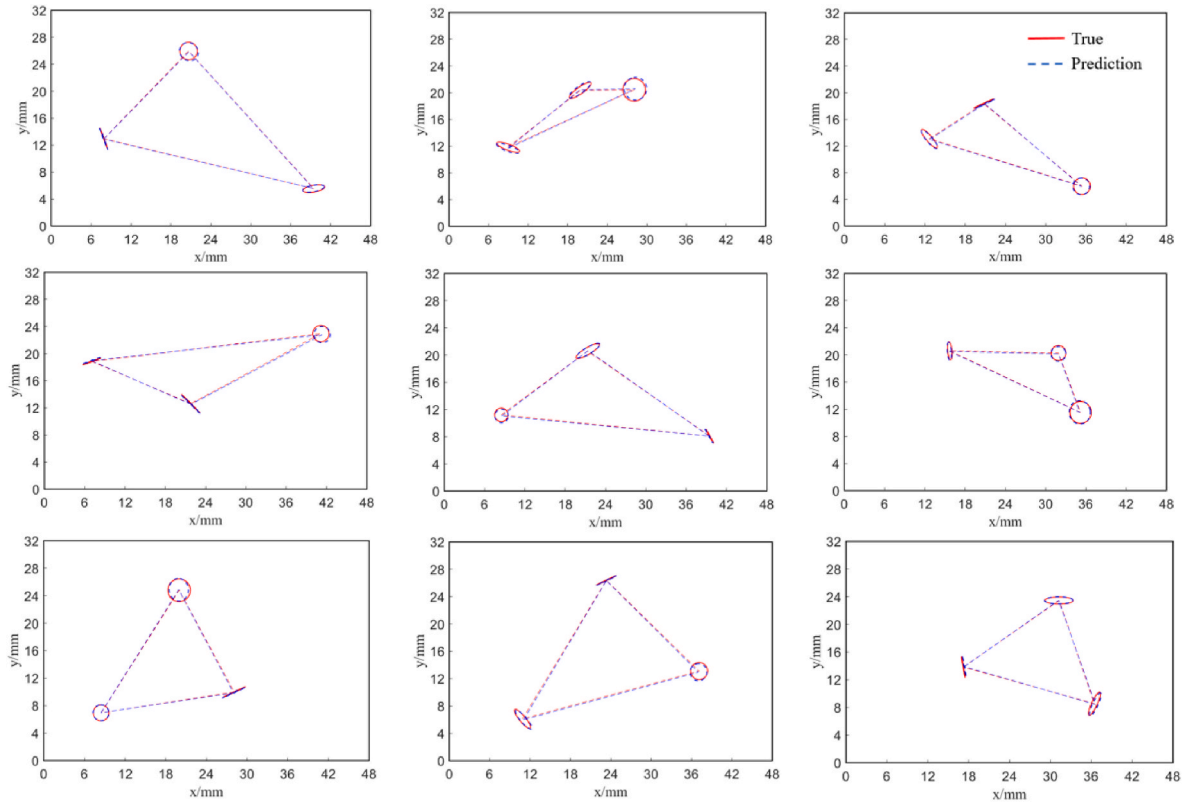

Fig. 23. Comparison between the true and prediction values for three random flaws.

2.2. A series connection NN model

In this analysis, a series connection artificial neural network (ANN) composed of classification and regression models is developed and constructed to achieve the damage identification. Deep neuron network (DNN) is one kind of ANN. It's a multi-layer structure with multiple labeled and feature data as well as hidden layers to enhance the expression ability of the model as expressed in Fig. 8.

The architecture of the classification and regression model is the same. Suppose there are totally l hidden layers in the DNN model. As a demonstration, the operation is nth layer, $n = 1, 2, \ldots, l$. The input and output of the layer are denoted by $h^{[n-1]}$ and $h^{[n]}$, respectively. Boundary strains $\boldsymbol{\epsilon}$ can be regarded as $h^{[0]}$. The output data is produced according to the equation as:

$$h_j^{[n]} = \sigma\left(\sum_k w_{jk}^{[n]} h_k^{[n-1]} + b^{[n]}\right), j = 1, 2, \ldots, D^{[n]}, \text{and } k = 1, 2, \ldots, D^{[n-1]} \quad (11)$$

where $D^{[n]}$ and $D^{[n-1]}$ are the number neurons of n and n-1 layer, respectively. w and b are the weight and bias parameters at the neuronal connections between adjacent layers which are the key problem to be determined in DNN models. The back propagation algorithm used in this model to effectively update the parameters to improve the accuracy of the complicated model. $\sigma(\cdot)$ is a non-linear function called the activation function. The training flow chart for DNN is shown in Fig. 9.

In this article, 2-D elastostatic problems are considered, the input is a 1-D array containing the boundary strains of points on the sensing network which can be obtained from a set of boundary strain gauges or numerical analysis. The output is the predicted feature data including damage number, location, geometry characteristics and classification.

2.2.1. The NN classification model

Classification NN model is one of the supervised machine learning algorithms. Its purpose is to find the decision boundary to make a qualitative analysis of the object and the output is the category to which

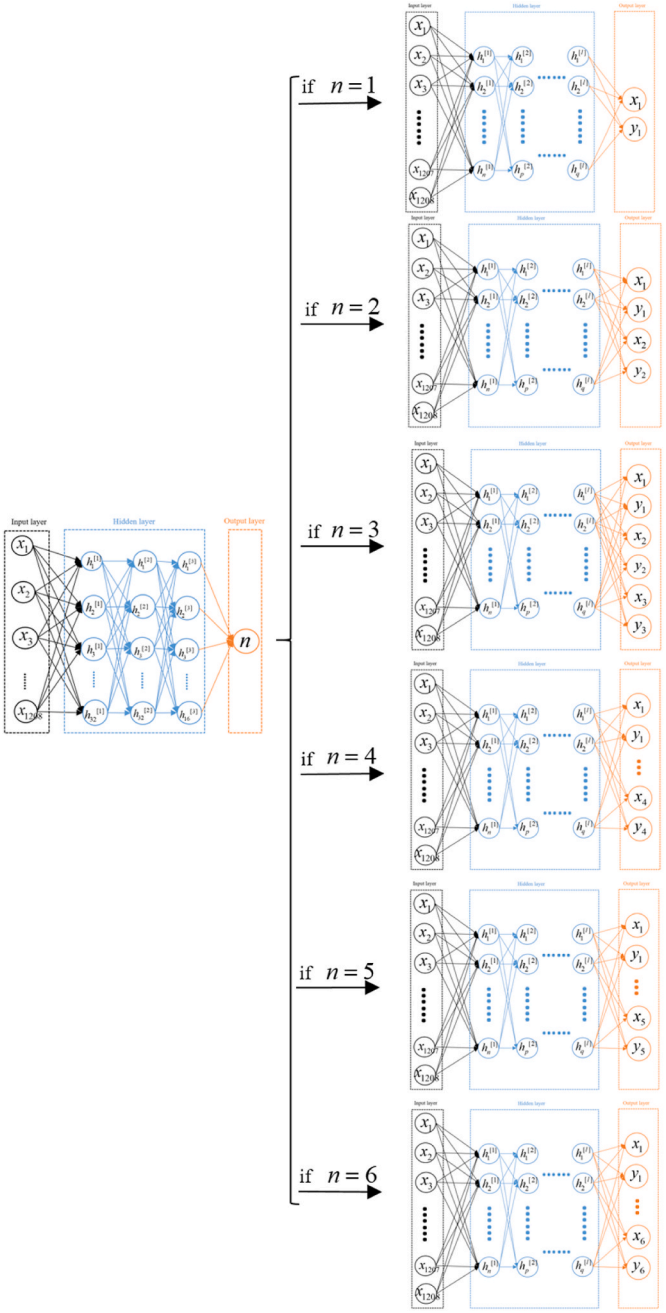

Fig. 24. Configuration of the series connection NN models for example five.

Table 9
NN parameters for example five.

Hidden layer number	Number of neurons	Parameters to be trained	Iterative steps	Accuracy rate	Training time/s
3	32-32-16	40374	100	0.9967	49

the object belongs. It can be used to deal with binary and multi-class classification problems. Thus, the classification NN model is employed to identify the number of the flaws.

In the training process, after collecting the dataset, the next important step is data preprocessing. Normalizing the data to the appropriate range can effectively improve the convergence speed of the algorithm, and avoid the gradient disappearance or gradient dispersion. In addition, it can reduce the scale differences between different features, making the model more stable and more robust. In this analysis, Z-Score normalization technique is employed to normalize the collected boundary strains to a range of mean 0 and variance 1. The new characteristics are normalized as:

$$\widehat{x}_i = \frac{x_i - \mu}{\sigma}, \text{ where mean } \mu = \frac{1}{n}\sum_{i=1}^{n} x_i \text{ and variance } \sigma^2 = \frac{1}{n}\sum_{i=1}^{n}(x_i - \mu)^2 \quad (12)$$

the classification model construction, the ReLU function is applied as the activation function for the first several layers to map the nonlinear relationship between neurons. About 50 % of the neurons using the ReLU function are activated, which is a good sparse NN, and the training process is more efficient. The ReLU equation and its image (Fig. 10 (a)) are listed below:

$$\mathrm{Re}LU(x) = \max(0, x) \quad (13)$$

Softmax function is the activation function for last layer of classification NN model to output the probability of the flaw numbers. Softmax is a generalization of logical function, and it can compress a K-dimensional vector $\mathbf{X}$ containing any real number into another K-dimensional vector, the range of each element is mapped to a probability real number between 0 and 1, and their sum is 1. The number which states the highest probability is predicted to be the realistic number of the flaws. Its equation and image (Fig. 10 (b)) are presented.

$$\sigma(x)_i = \frac{e^{x_i}}{\sum_{i=1}^{K} e^{x_i}} \quad (14)$$

The corresponding Cross Entropy Loss function is employed as loss function to measure the variability in the probability distribution.

$$Loss = -\sum_{i=0}^{C-1} y_i \log(p_i) \quad (15)$$

where C represents the number of sample categories, y_i is the one-hot representation of the sample labels. i.e., when the sample belongs to the i-th category, is, $y_i = 1$, otherwise $y_i = 0$. p_i indicates the probability that the sample is in class i.

In the back propagation algorithm, the final loss value back-propagates from the last layer to the front layer, and calculates the derivatives of the weights and bias in the network. The optimization process of NN is essentially the process of updating the weight and bias so as to minimize the objective function $Q(w)$. Assuming that n samples exist, the objective function can be written in the following form:

$$Q(w) = \frac{1}{n}\sum_{i=1}^{n} Q_i(w) \quad (16)$$

In this process, the Adam is employed to optimize the NN parameters. Its equation is:

$$\begin{aligned} m &:= \frac{\beta_1 m + (1-\beta_1)\nabla\widehat{Q}(w)}{1-\beta_1}, \nabla\widehat{Q}(w) = \frac{1}{m}\sum_{i=1}^{m}\nabla Q_i(w) \ , \\ v &:= \frac{\beta_2 v + (1-\beta_2)\nabla\widehat{Q}(w)}{1-\beta_2} \ , \\ w &:= w - \eta\frac{m}{\sqrt{v}+\kappa} \ , \end{aligned} \quad (17)$$

where m is the number of random samples, where mini-batch size is 32. η represents learning rate. β_1 and β_2 are momentum parameters to make the algorithm more stable. κ generally takes a very small positive number. In the training process, small batch can effectively reduce computation time and memory consumption, and can reach convergence faster, make the model more stable. In addition, it can effectively avoid the local optimal solution, due to randomly selected each small

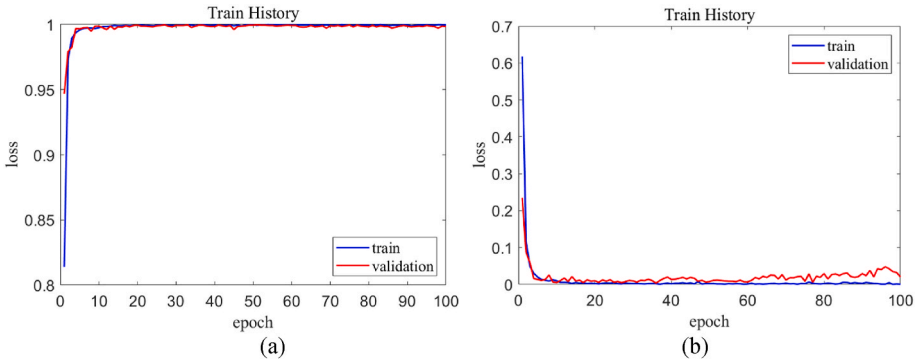

Fig. 25. Convergence processes of example five NN model (a) accuracy, (b) loss value.

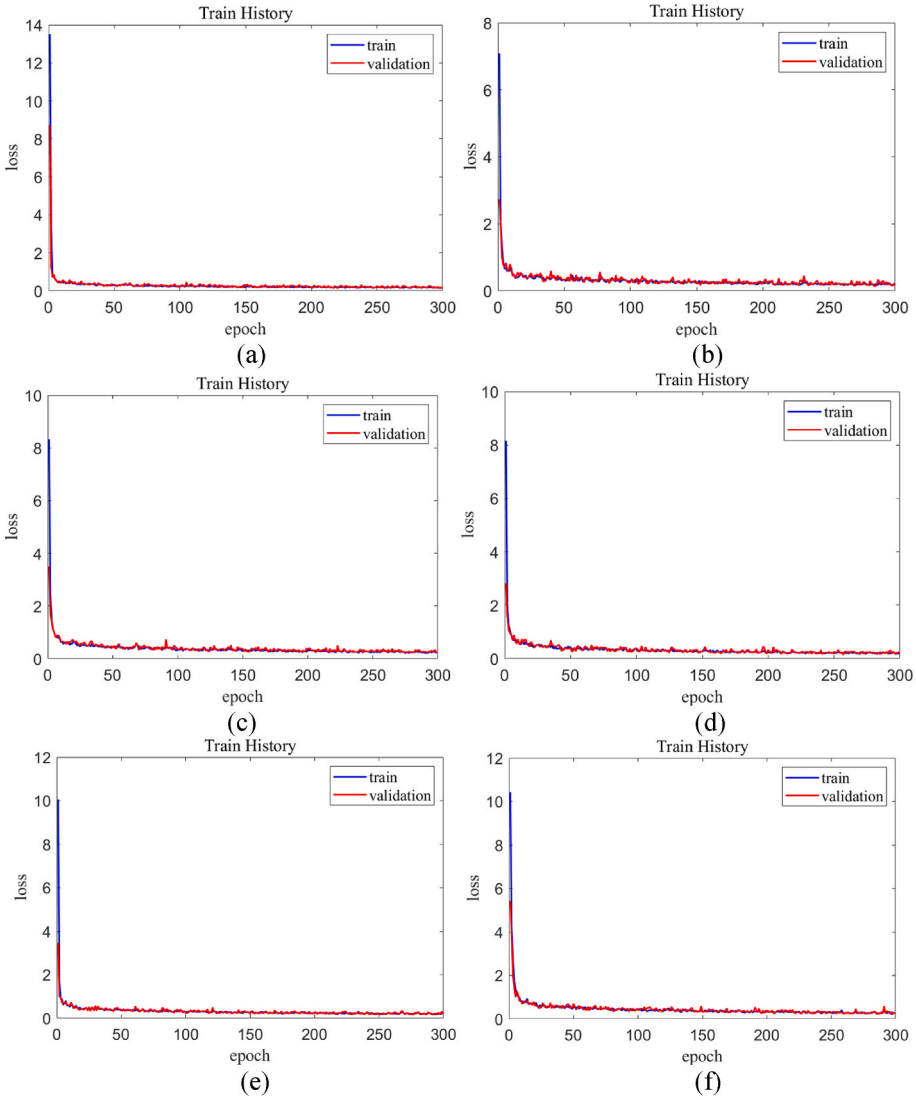

Fig. 26. Convergence processes of example five NN model with flaw number of (a) 1, (b) 2, (c) 3, (d) 4, (e) 5, (f) 6.

batch can explore more parameter space.

Last but not least, for the reason of the complex model and the relatively small dataset, during training a DNN, it is easy to overfit the noise and randomness of the training data to form an overfitting model. Network regularization can reduce the complexity of the model by limiting the model parameters to reduce the risk of overfitting. Dropout is one kind of regularization techniques by randomly deleting some neurons with a certain probability, the dependence between neurons can be reduced, thus reducing the risk of overfitting. In this study, the randomly discarded proportion is set to 30 % when the constructed network structure is above 3 hidden layers and the number of single-layer neurons is large.

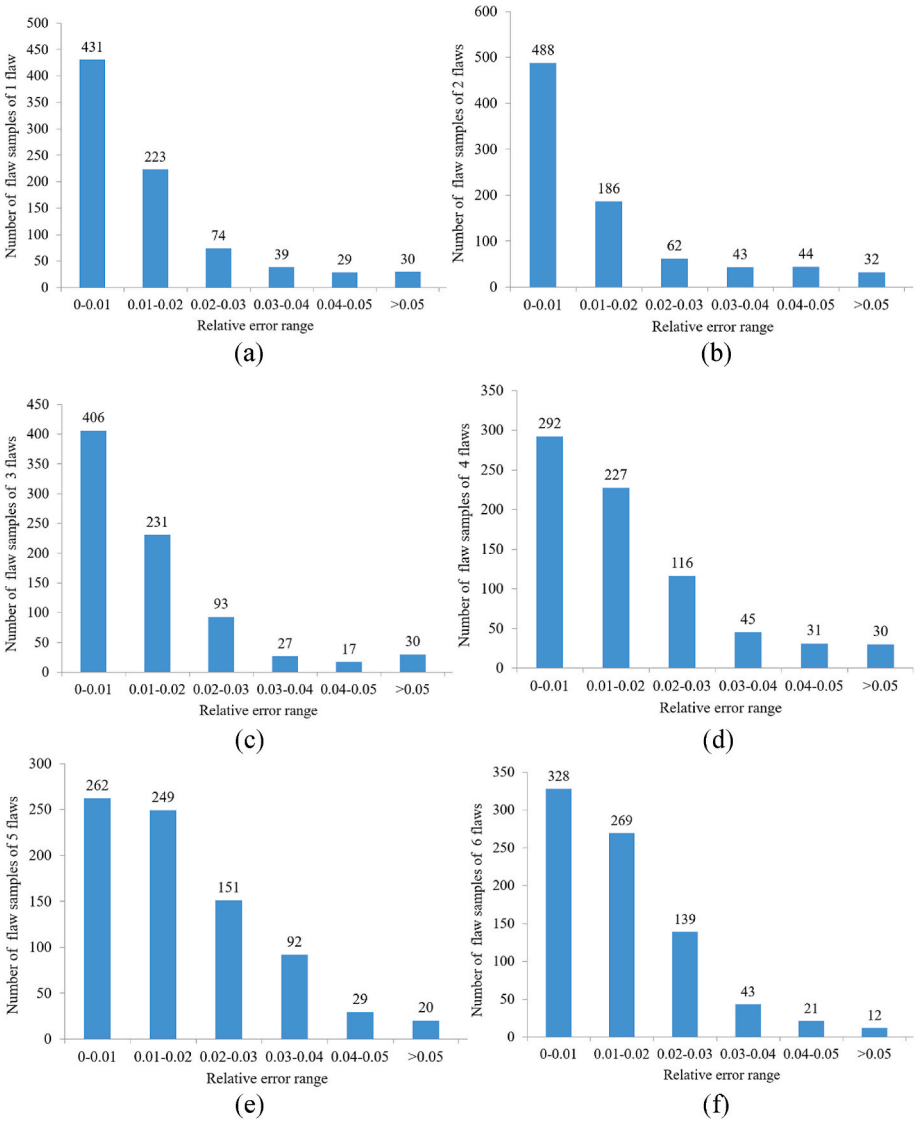

Fig. 27. Loss value range of testing samples for example five with flaw number of (a) 1, (b) 2, (c) 3, (d) 4, (e) 5, (f) 6.

2.2.2. *The NN regression model*

Regression NN model is also one of the supervised machine learning algorithms. Its purpose is to find the optimal fitting value to approach the real value to make a quantitative analysis of object. After determining the number of flaws, the NN regression model is applied to predict the detailed location and geometric characteristics for each flaw.

In regression model, ReLU function is applied as the activation function for all of the layers to map the nonlinear relationship between neurons. To measure the deviation between the prediction value and the true value, the Mean Absolute Error (MAE) is adopted as the loss function. It will be more robust in the presence of outliers.

$$MAE = \frac{1}{N}\sum_{i=1}^{N}|y_{iTrue} - y_{iPred}| \tag{18}$$

where y_{iTrue}、 y_{iPred} represent the true and prediction value for i-th data, respectively. The same as classification model, mini-batch size is 32. Adam optimizer is employed to optimize the NN parameters. Dropout regularization is used to reduce the risk of overfitting. Z-Score normalization technique is employed to normalize the collected boundary strains to a range of mean 0 and variance 1.

One thing needs to be noticed that, the output of the regression model includes the Cartesian coordinates of center, radius or axis length, and the angles. They belong to different dimensions. A normalization step is necessary to be used to deal with the feature data to improve the convergence speed. Max-Min Normalization is employed to scale the feature data to [0, 1] or [−1, 1] interval. The other values are mapped to the corresponding interval through linear transformation by

$$\widehat{x}_i = \frac{x_i - x_{\min}}{x_{\max} - x_{\min}} \tag{19}$$

After obtaining the predicted feature data, a back normalization technique is used to recover their corresponding realistic values.

The flowchart of the present algorithm is depicted in Fig. 11.

3. Numerical examples

In this analysis, several examples of a plate with random damages in the form of circular, elliptical holes and cracks are considered. For the sake of computation, the geometry, material properties, boundary and loading conditions as well as mesh distributions of the plate and flaws are consistent with the verification examples.

3.1. *A plate with two circular holes*

Location and extent functionalities of the present damage detection

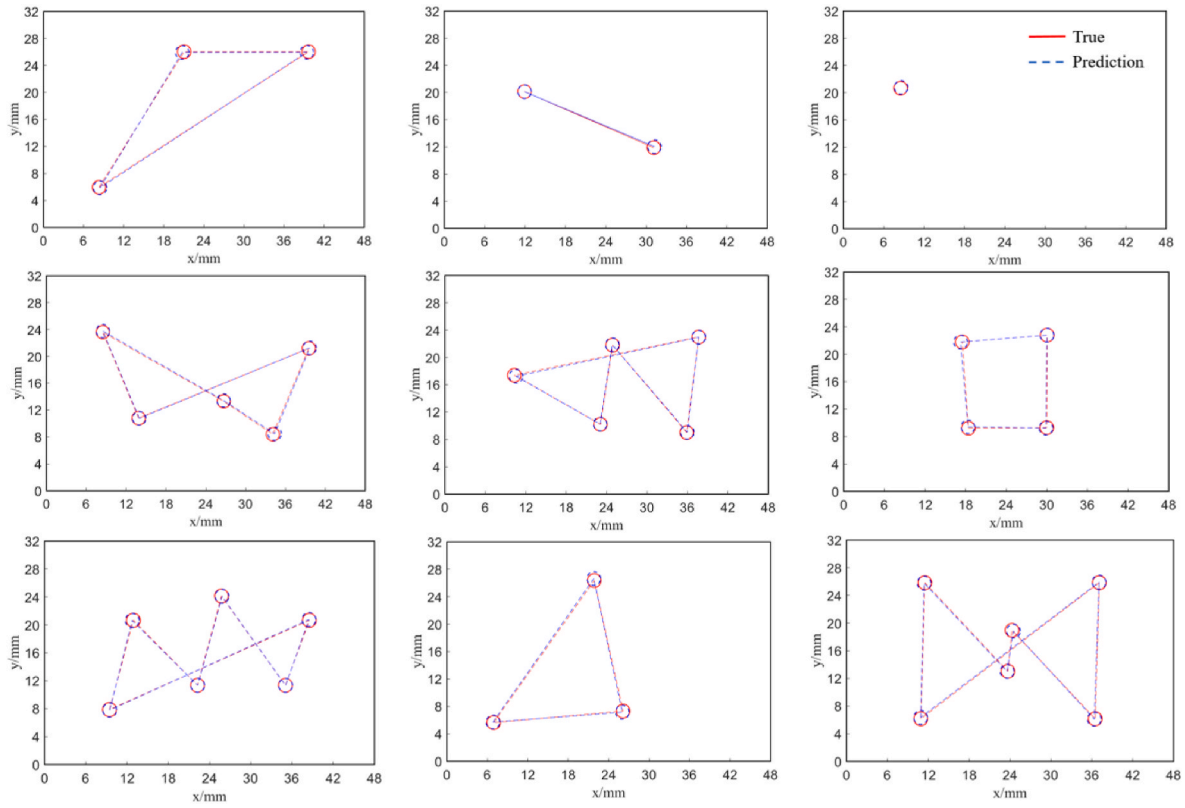

Fig. 28. Comparison between the true and prediction values for the circular holes with random number.

algorithm are first evaluated. A plate subjected to remote stress having two circular holes with different radii, as shown in Fig. 12, is proposed. A total number of 604 constant elements are employed to discretize the edges of the plate and each edge of the flaws is discretized into 100 constant elements. For this example, the strains at each boundary node of the plate are the input while the center coordinates and radius of these two circular holes are exported.

Data are collected by moving the center of the circular hole along x and y axes inside the range of the plate, and the radius of each circular flaw varies from 1.0 to 2.5 mm. By random combining these parameters, a highly qualified dataset with a total of 5625 samples is established, in which a large number of repetitive data sets is avoided to prevent the occurrence of non-unique results, as well as overlapping flaws are also forbidden. With randomly shuffled the samples, 3937 samples account for 70 % are used for training the network, and the left 30 % samples are employed for testing. Among of several optimal NN models, a 64-64-32 configuration is confirmed to be the optimized model and the detail parameters of this model are listed in Table 5.

The convergence process of loss value can be found in Fig. 13 (a). After 100 epochs, the loss value tends to be a constant until achieves 0.03 cm at the end. Thus, the model is considered to have good generalization ability and can be used for testing. A total of 1688 samples have been tested by the proposed model, over 90 % of samples have a relative error less than 0.05 %. The range of the relative error distribution of the testing samples are tabulated in Fig. 13 (b).

Three random prediction results of testing samples are plotted in Fig. 14 which are compared with the true flaws. High degree of consistency between the predictions and true values demonstrates the efficiency of the proposed algorithm.

3.2. Two random elliptical holes in a plate

The classification ability of the present algorithm is verified by through prognosis different shape flaws in a plate. First, the plate with two elliptical flaws having different long, short axes and angles between the long axis and longitudinal direction is plotted in Fig. 15 and investigated.

Data is collected by moving the coordinates of each flaw center along x and y axes inside the range of the plate. The lengths of semi-long and short axes vary in the range of 2.0 mm–4.0 mm and 1.0 mm–2.0 mm, respectively. Meanwhile, the angle between x-axis and long axis varies from 0 to 180°. By randomly combing these parameters, a total number of 6100 date sets are collected without date duplicating and flaws overlapping. A regression NN construction with three hidden layers is applied to predict the elliptical flaws, the detail parameters are listed in Table 6. The input data is still the boundary strains of the plate. One should be noted that the output neurons have non-homogeneous dimensionally which include length and angle. Thus, the predicted values are first normalized by the max-min normalization and linearly transformed into the scale between (0, 1). Then, a reverse normalization step is employed to return the realized values to the output neurons.

The model converges quickly as shown in Fig. 16 (a), after 100 epochs, the loss value finally achieves 0.0076. The statistics of relative error for the testing samples are tabulated in Fig. 16 (b) which presents the high generality of the model. The predictions of location, classification, extent of two elliptical holes in a plate are matched well with that of the true flaws and depicted in Fig. 17.

3.3. Two random cracks in a plate

With the length of short axis getting over to 1/10 of the long axis length, an elliptical flaw becomes to be a crack which is a ubiquitous form of the defect existence. Thus, cracks with different lengths and angles between length and longitudinal direction in a plate are also studied and depicted in Fig. 18.

Data is collected by moving the coordinates of center point of the cracks along x and y axes inside the range of the plate. Vary the crack lengths from 2.0 mm to 4.0 mm as well as the angles between crack and

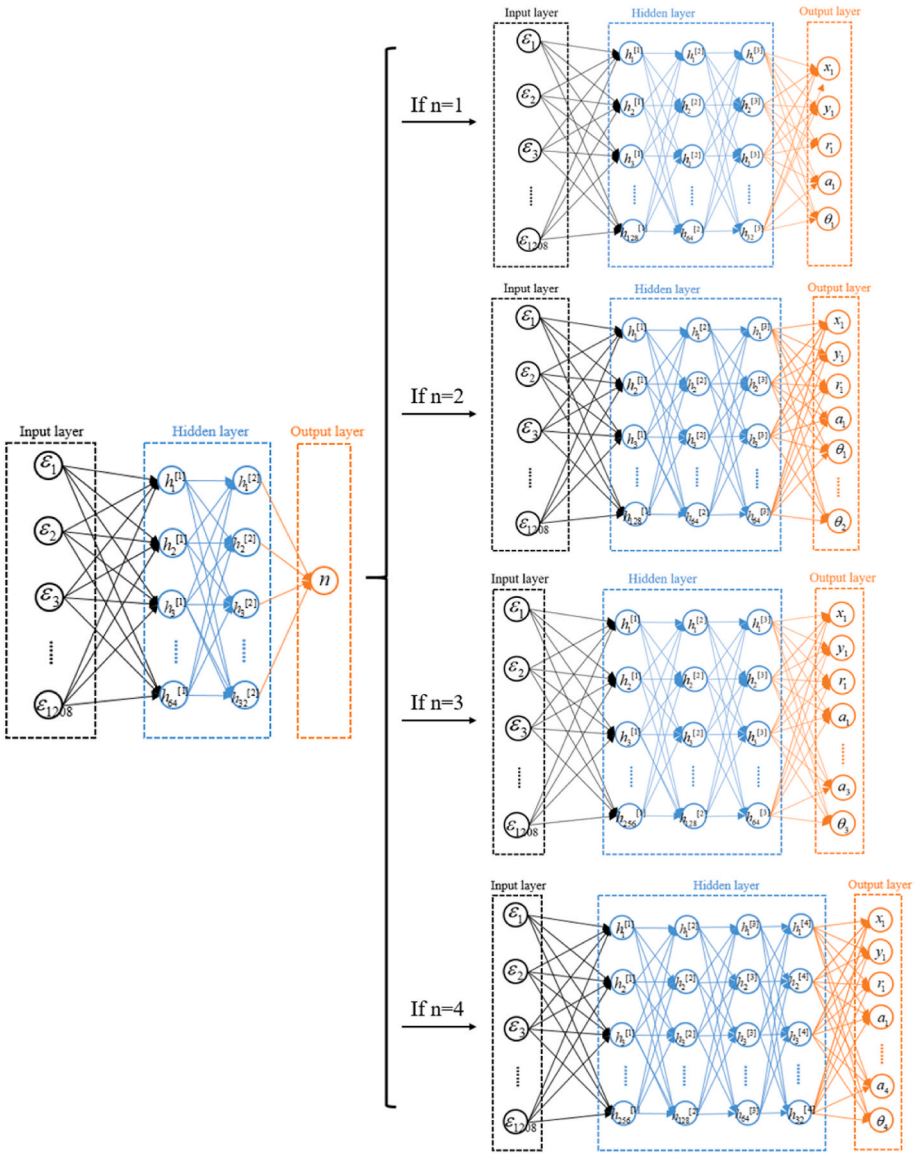

Fig. 29. Configuration of the series connection NN models for example six.

Table 10
NN parameters for example six.

Hidden layer number	Number of neurons	Parameters to be trained	Iterative steps	Accuracy rate	Training time/s
2	64–32	79588	100	0.9986	45

the x-axis from 0 to 180°. A total number of 5000 datasets is built without duplicated data and overlap flaws. The same strategy algorithm as elliptical flaw is employed. An optimal NN structure with four hidden layers is constructed and the detailed parameters are listed in Table 7.

Fig. 19 (a) shows the convergence process of this model, after 150 epochs, the loss value converges to 0.0078. The statistics of relative error for the testing samples in Fig. 19 (b) and the comparison between the predictions and true flaws in Fig. 20 all illustrate the high prediction ability of the present algorithm.

3.4. Three random flaws in a plate

A plate with three flaws in the form of circular, elliptical holes and cracks as shown in Fig. 21 is investigated by the present algorithm.

The same loading condition is subjected on the plate. By randomly combing the parameters for each flaw, a dataset with a total number of 5292 is collected which avoids the duplicated data and overlap flaws. The output neurons include the location of the flaw center, the radius or the long, short axes and angles for each flaw. 70 % of the data are used for training. Finally, an optimal NN model with four hidden layers is constructed and the detailed parameters are shown in Table 8.

From the convergency figure (Fig. 22 (a)) it can be observed that after 200 steps, the loss values tend to converge and finally achieve 0.0084. Thus, this mode is believed to possess good generalization and can be applied to predict the flaws. The relative error of total 1847 testing samples are counted and tabulated in Fig. 22 (b). Over 90 % of samples achieve a relative value of less than 3 %. The comparisons between prediction results and true flaws of nine random samples are described in Fig. 23. The high consistency illustrates the developed algorithm has high efficiency in localization, classification and description of damage detection.

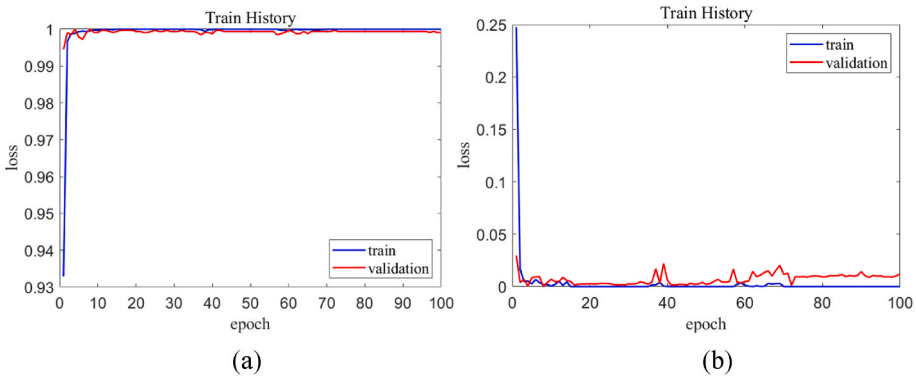

Fig. 30. Convergence processes of NN model for example six (a) accuracy, (b) loss value.

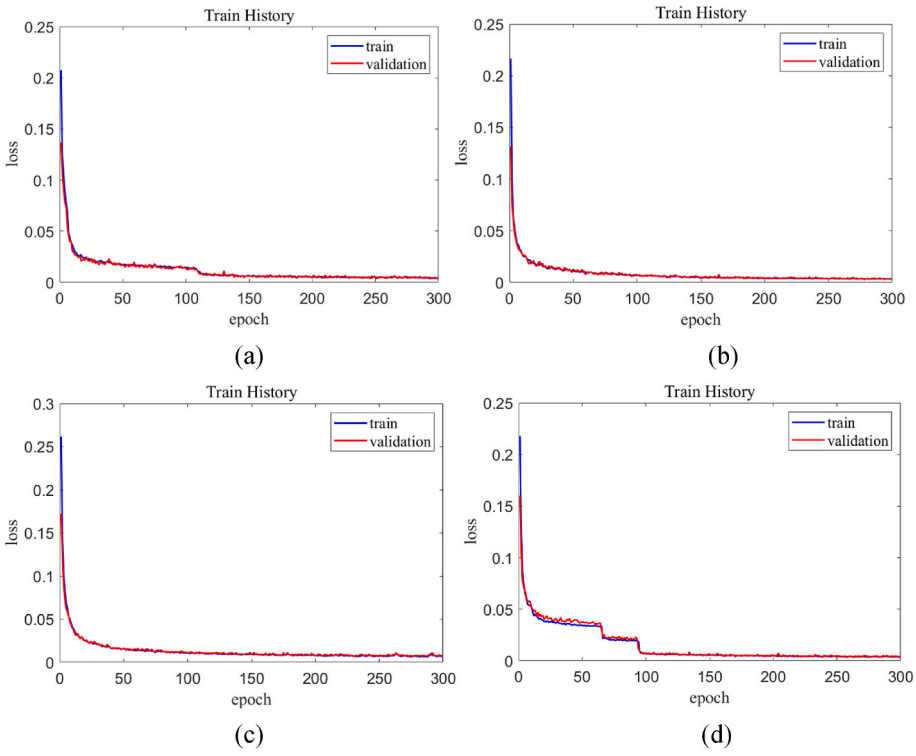

Fig. 31. Convergence processes of example six NN model with flaw number of (a) 1, (b) 2, (c) 3, (d) 4.

3.5. A plate with unknow number of circular holes

For determining the number of flaws, a series connection neural network is constructed and its configuration is plotted in Fig. 24. At First, a classification NN configuration is built to analyze the number of flaws, where the output neuron has only one. After making sure the number of flaws, an indicator points to the corresponding regression NN model and transmits the extracted features to prognosis the detailed location, classification and extent of the flaws, where the number of output neurons for each regression NN model is different. A plate with unknown number of circular holes is predicted to demonstrate the algorithm. By combing the number and the characteristic parameters of circular holes, an abundant dataset with a total number of 24204 is produced. The dataset is comprised of six groups' data with different number of flaws from one to six. After random shuffled the data, 80 % among of them are used for training the model and 20 % residue are used for testing.

A classification NN with three hidden layers is constructed and the detailed information is listed in Table 9. Softmax is chosen as the activation function for the output layer to predict the probability of numbers. The number with the highest value of probability is selected as the number of flaws, while, the Cross Entropy loss is employed to value the accuracy. After determining the number of the circular holes, the number as an indicator points to the corresponding regression NN model and the next process of detailed prediction for each flaw is the same as before and omitted here.

At the first step for flaw number prognosis, the convergence processes of accuracy and loss value are shown in Fig. 25. After 20 epochs, the model begins to converge and finally achieves 99.67 % precision. Thus, the model is believed with high generality to predict the number as well as the detailed information of studied flaws.

The convergency processes of loss value for the sequential regressive NN models are depicted in Fig. 26. In which, figures (a)–(f) represent the regressive NN model for predicting the flaw numbers from 1 to 6,

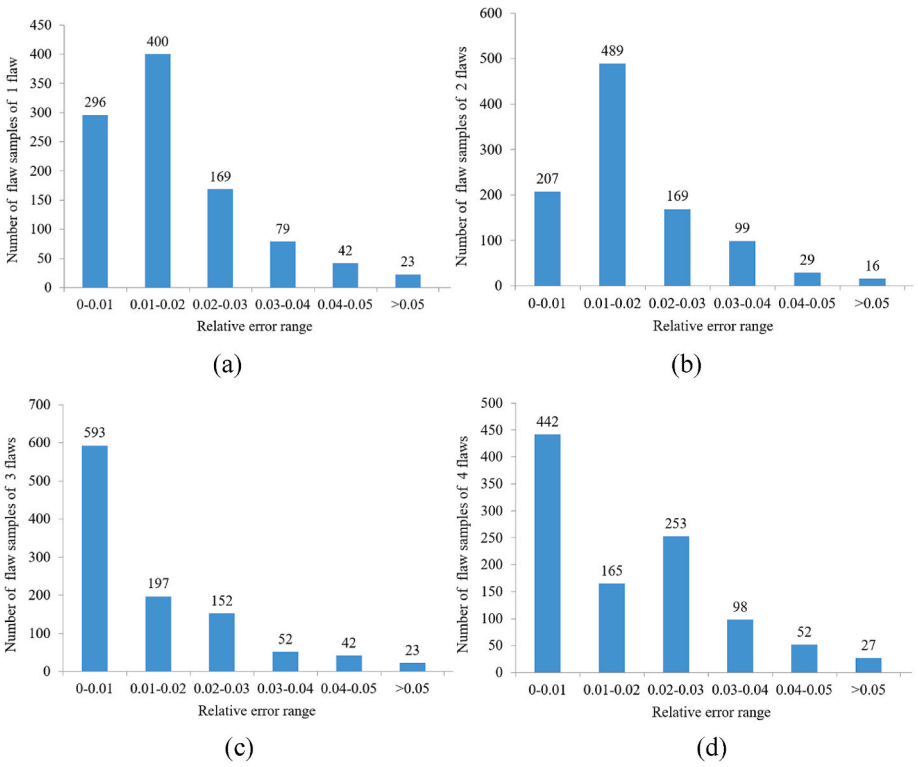

Fig. 32. Loss value range of testing samples for example six with flaw number of (a) 1, (b) 2, (c) 3, (d) 4.

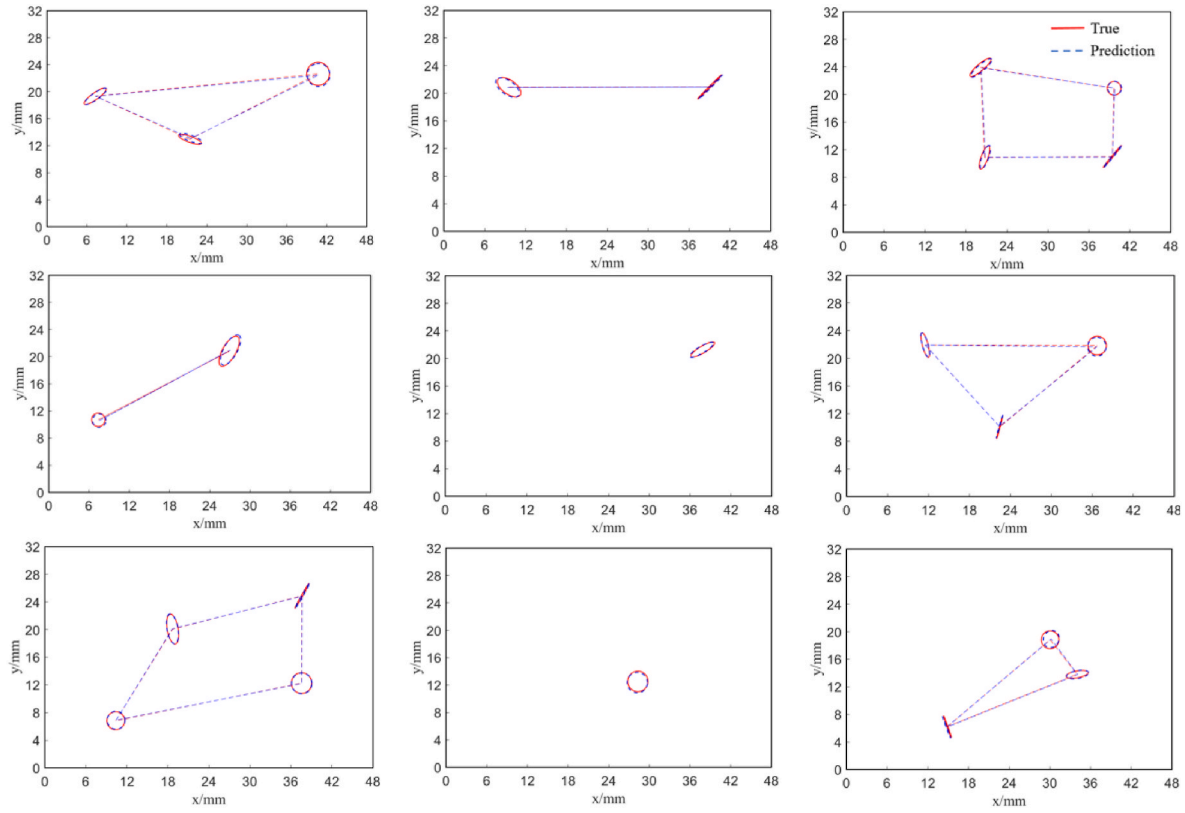

Fig. 33. Comparison between the true and prediction values for the flaws with random number.

respectively. Their corresponding relative errors for the testing samples are also plotted in Fig. 27, respectively. Based on the results, over 95 % samples have the relative errors below 5 % in the damage detection.

The predicted geometry information for random number of circular holes is compared with the true one. Nine random testing samples are plotted in Fig. 28. It can be concluded that the series connection NN

algorithm owns high accuracy to prognosis the number, location and extent of the circular holes.

3.6. A plate with random number and type flaws

At last, a finally series connection NN model to prognosis the number, location, classification, extent of the flaws is developed. Its efficiency is demonstrated by the example of a plate with random number and flaws in the form of circular, elliptical holes and cracks. The loading condition and material properties of the plate are considered the same as in previous cases. By randomly combing the characteristic parameters of the flaws, a total number of 20562 datasets including the number of flaws from one to four is collected. After random shuffled the samples, 80 % of them are used for training and the left are used for testing.

The configuration of the series connected NN model is described in Fig. 29. Similarly, the target of the first classification NN model is to determine the exact number of the flaws. Then, an indicator transforms the extracted features into a corresponding regression NN model to predict the detailed characteristics of the flaws. A two hidden layer classification NN model is constructed. Softmax function is adopted as the activate function for the output neurons to determine the number probability. Cross Entropy is employed as the loss function. The strategy of the regression NN model is similar to the previous one and omitted here.

For the first classification NN model, the detailed parameters are listed in Table 10. The accuracy and convergence process versus epoch are plotted in Fig. 30. After 20 epochs, the model tends to converge, and the testing accuracy can achieve 99.86 %.

The convergence process of loss value for the sequential regression NN models for predicting the flaws number from one to four are depicted in Fig. 31 respectively. The loss value distributions of the testing samples are tabulated in Fig. 32. The loss values of 85 % samples are within 0.03. The predicted results of nine random samples are compared with that of true flaws and presented in Fig. 33. It can be concluded that the number, location, classification, extent of the flaws can be predicted accurately by the developed algorithm.

4. Conclusions

A novel damage identification approach based on the BE model-driven and NN data-driven combined algorithm is developed in this paper. By using only boundary strains of the considered structure, the existence, location, classification as well as the extent of the damage can be predicted at once with high accuracy and efficiency.

One important aspect of the high accuracy and efficiency is due to a high-quality dataset with generalizability, fairness and scientific validity which created by a model-driven algorithm. In this approach, BEM is taken as the tool for designing an optimal SHM sensor network and a data-base creator to construct the training dataset. Data compression is one of the important stages to decrease the label number and is implemented by using the BEM with its dimensionality reduction characteristic. The reduction in the quantity of dataset does not reduce the data quality due to the semi-analytical nature of the BEM. By randomly combing the parameters of the damage, large dataset is constructed by using the BEM simulation for which only the boundary strains are needed. This data can also be collected from the experimental data by using strain gauges on the boundary.

Then, a series connection NN model is developed to construct the exact mapping relationship between deformation and configuration of the structure. Six different kinds of examples demonstrate the high efficiency and accuracy of the present method to predict the damage number, location, classification and extent. A high accuracy of about 99.86 % is achieved by the present combined neural network algorithm, which is promising in applications of the actual structural health monitoring.

CRediT authorship contribution statement

Yang Yang: Writing – review & editing, Writing – original draft, Supervision, Methodology, Conceptualization. **Zheng Zhan:** Data curation. **Yijun Liu:** Writing – review & editing, Supervision.

Declaration of competing interest

The authors declare that they have no known competing financial interests or personal relationships that could have appeared to influence the work reported in this paper.

Data availability

Data will be made available on request.

Acknowledgments

The authors would like to thank the financial support from the National Natural Science Foundation of China (Project Nos. 12272160 and 11972179).

References

Alamdari, M.M., Rakotoarivelo, T., Khoa, N.L.D., 2017. A spectral based clustering for structural health monitoring of the Sydney harbor bridge. Mech. Syst. Signal Process. 87, 384–400.
Bigoni, C., Hesthaven, J.S., 2020. Simulation-based anomaly detection and damage localization: an application to structural health monitoring. Comput. Methods Appl. Mech. Eng. 363, 112896.
Bolandi, H., Li, X., et al., 2022. Bridging finite element and deep learning: high-resolution stress distribution prediction in structural components, 16, 1365–1377.
Cao, P., Qi, S., Tang, J., 2018. Structural damage identification using piezoelectric impedance measurement with sparse inverse analysis. Smart Mater. Struct. 27, 035020.
Fang, X., Luo, H., Tang, J., 2005. Structural damage detection using neural network with learning rate improvement. Comput. Struct. 83, 2150–2161.
Farrar, C.R., Worden, K., 2007. An introduction to structural health monitoring. Philosophical transactions of the Royal Society. Mathematical, Physical, and Engineering Sciences 365 (1851), 303–365.
Figueiredo, E., Gyuhae, P., et al., 2011. Machine learning algorithms for damage detection under operational and environmental variability. Struct. Health Monit. 10 (6), 559–572.
Gonzalez, M.P., Zapico, J.L., 2008. Seismic damage identification in buildings using neural networks and modal data. Comput. Struct. 86 (3–5), 416–426.
Han, X.Y., Yang, Y., Liu, Y.J., 2022. Determining the defect locations and sizes in elastic plates by using the artificial neural network and boundary element method. Eng. Anal. Bound. Elem. 139, 232–245.
Hekmati Athar, S.P., Taheri, M., Secrist, J., et al., 2020. Neural network for structural health monitoring with combined direct and indirect methods. J. Appl. Remote Sens. 14 (1), 1.
Jagtap, A.D., Kharazmi, E., Karniadakis, G.E., 2020. Conservative physics-informed neural networks on discrete domains for conservation laws: applications to forward and inverse problems. Comput. Methods Appl. Mech. Eng. 365, 113028.
Jin, Q., Liu, Z., Bin, J., et al., 2019. Predictive analytics of in-service bridge structural performance from SHM data mining perspective: a case study. Shock Vib. 2019, 1–11.
Jung, J., Taciroglu, E., 2014. Modeling and identification of an arbitrarily shaped scatterer using dynamic XFEM with cubic splines. Comput. Methods Appl. Mech. Eng. 278, 101–118.
Kassab, A.J., Moslehy, F.A., Daryapurkar, A.B., 1994. Nondestructive detection of cavities by an inverse elastostatics boundary element method. Eng. Anal. Bound. Elem. 13 (1), 45–55.
Ku, K., Silva, K.E., Yoon, G., 2023. Statistical topology optimization scheme for structural damage identification. Comput. Struct. 286, 107094.
Lee, S.-H., Song, J., 2016. Bayesian-network-based system identification of spatial distribution of structural parameters. Eng. Struct. 127, 260–277.
Li, Z.X., Yang, X.M., 2008. Damage identification for beams using ANN based on statistical property of structural responses. Comput. Struct. 86 (1–2), 64–71.
Liu, Y.J., 2009. Fast Multipole Boundary Element Method - Theory and Applications in Engineering. Cambridge University Press, Cambridge.
Lu, Q., Zhu, J., Zhang, W., 2020. Quantification of fatigue damage for structural details in slender coastal bridges using machine learning-based methods. J. Bridge Eng. 25 (7), 04020033.
Malekloo, A., Ozer, E., Alhamaydeh, M., et al., 2022. Machine learning and structural health monitoring overview with emerging technology and high-dimensional data source highlights. Struct. Health Monit. 21 (4), 1906–1955.

Mariniello, G., Pastore, T., et al., 2020. Structural damage detection and localization using decision tree ensemble and vibration data. Comput. Aided Civ. Infrastruct. Eng. 36 (9), 1129–1149.
Mellings, S.C., Aliabadi, M.H., 1993. Dual boundary element formulation for inverse potential problems in crack identification. Eng. Anal. Bound. Elem. 12 (4), 275–281.
Mitusch, S.K., Funke, S.W., Kuchta, M., 2021. Hybrid FEM-NN models: combining artificial neural networks with the finite element method. J. Comput. Phys. 446, 110651.
Moore, E.Z., Nichols, J.M., Murphy, K.D., 2012. Model-based SHM: demonstration of identification of a crack in a thin plate using free vibration data. Mech. Syst. Signal Process. 29, 284–295.
Salehi, H., Biswas, S., Burgueno, R., 2019. Data interpretation framework integrating machine learning and pattern recognition for self-powered data-driven damage identification with harvested energy variations. Eng. Appl. Artif. Intell. 86, 136–153.
Sohn, H., Farrar, C.R., Hemez, F.M., et al., 2003. A Review of Structural Health Monitoring Literature: 1996–2001. LA-13976-MS. Los Alamos National Laboratory, Los Alamos, NM.
Sun, H., Waisman, H., Betti, R., 2016. A sweeping window method for detection of flaws using an explicit dynamic XFEM and absorbing boundary layers. Int. J. Numer. Methods Eng. 105 (13), 1014–1040.
Sun, L., Shang, Z., et al., 2020. Review of bridge structural health monitoring aided by big data and artificial intelligence: from condition assessment to damage detection. J. Struct. Eng. 146 (5), 04020073.
Sun, J., Liu, Y., Yao, Z., et al., 2022. A data-driven multi-flaw detection strategy based on deep learning and boundary element method. Comput. Mech. 1–26.
Wang, L., Zhou, J., Lu, Z.R., 2020. A fast friction-model-inspired sparse regularization approach for damage identification with modal data. Comput. Struct. 227, 106142.
Xu, Z.L., 2016. Elasticity. Higher Education Press.
Yang, Y., Kou, K.P., et al., 2015. Free vibration analysis of two-dimensional functionally graded coated and undercoated substrate structures. Eng. Anal. Bound. Elem. 60, 10–17.
Yang, D., Yi, C., Xu, Z., et al., 2017. Improved tensor-based singular spectrum analysis based on single channel Blind source separation algorithm and its application to fault diagnosis. Appl. Sci. 7 (4), 418.
Yang, X.W., Li, Z.X., et al., 2023. Mining graph-based dynamic relationships for object detection. Eng. Appl. Artif. Intell. 126, 106928.
Zhang, Q.W., 2007. Statistical damage identification for bridges using ambient vibration data. Comput. Struct. 85 (7–8), 476–485.